4
Zn Interstitial Defects and Their Contribution as Efficient Light Blue Emitters in Zn Rich ZnO Thin Films

4.1 Introduction

ZnO has wide band gap and intrinsic n-type characteristics. It is one of the oldest oxide compound semiconductors and has attracted the resurgent interest of electronic industries for different applications. ZnO is a good candidate for white lightening. Although ZnO has several advantages, the inability to have control over defects and dopants puts a restrictions over practical realization of devices. It is an important aspect to analyse the defects present in any semiconductor before using it for any application as defects affect the physical properties and is responsible for some intrinsic properties of materials as well. These defects facilitate self as well as impurity diffusion and hence affect materials' growth directly or indirectly, processing, and device efficiency (Janotti and Van de Walle, 2007a). Zinc oxide has several point defects but oxygen vacancies and zinc interstitials are such two point defects which have been often mentioned as a basis of n-type conductivity of ZnO. However, there is no direct conclusive evidence available to support this statement but diffusion studies of defects and its impact on electrical conductivity along with Hall measurements may be regarded as the evidence (Janotti and Van de Walle, 2007a). These defects have effects on photoluminescence as well which is well observed in PL spectra showing a broad defect range in visible region. Hence understanding these defects are crucial in order to successful implementation of devices for different applications. Oxygen vacancies and its effect on the properties of zinc oxide are reported by both experimental and theoretical calculations. However, Zinc interstitial is another defect which has not been investigated prominently to study its effect on properties of zinc oxide, experimentally.

Placing excess zinc in ZnO can either occupy the antisite or interstitial positions. The zinc interstitials have lower formation energy with respect to antiste and hence, are more favourable during synthesis. Zinc interstitials behave as shallow donors in ZnO system as reported by first principle calculations (Janotti and Van de Walle, 2007a). Zinc interstitials are present in +2 charge state in ZnO and indeed will transfer the electrons to conduction band and thus, acts as shallow donor. Defects are also produced in ZnO by electron irradiation at lower temperatures and measured by optically detected magnetic resonance (ODMR) measurements (Vlasenko and Watkins, 2005). The g factor of 1.96 is reported which tends to disappear after 170 K. The theoretically reported migration barriers are low ~ 0.57 eV indicating that these are fast diffusers. There are two interstitial positions available in hexagonal wurtzite structure of ZnO i.e. tetrahedral and octahedral voids. The tetrahedral site in ZnO has one of each zinc and oxygen atoms as nearest neighbour atoms with a distance around 0.833 times distance of Zn-O bond length(Janotti and Van de Walle, 2009). In octahedral void, three zinc and three oxygen atoms are nearest neighbour and is equidistance by 1.07 times the bond length of Zn-O. The energy of zinc interstitials in tetrahedral void is 0.9 eV higher than octahedral void, hence, placing the zinc interstitial atoms in tetrahedral site will lead to instability and severe constrains in lattice of ZnO. This shows that the interstitial zinc atoms will reside in octahedral void which

has the atomic radius equivalent to zinc radius (0.74 Å). Thus, the understanding of these defects on various properties of ZnO is required in order for use in further applications.

This chapter reports a simple synthesis technique of excess zinc containing zinc oxide (Zn:ZnO) along with pristine ZnO thin films to study the impact of excess zinc on the structural, microstructural, optical, emission, and electrical properties of ZnO. The structural studies substantiate the presence of excess zinc in octahedral void along with excess electron carrier concentration with Burstein-Moss shift of 0.13 eV in CB. The emission spectra of zinc rich film showed higher intensity in defect related emission substantiating the presence of interstitial zinc atom.

4.2 Experiments

We used n-type (111) oriented silicon substrates for depositing ZnO and Zn:ZnO thin films. Prior to any deposition, the substrates are cleaned using standard RCA1 and RCA2 cleaning procedure. The substrates are then subjected to diluted hydrofluoric acid (HF) solution to remove oxide layers present on the surface. The hydrophobic substrates are then washed in DI and dried using nitrogen gas. Thin gold film (10 nm) is deposited on clean substrates using thermal evaporation technique, which acts as the catalyst to facilitate VLS growth of films (Kumari et al., 2018a). A CVD furnace with three temperature zones is used for growth of these films. This CVD system has an inlet and outlet for inert/reactive gas flow inside the system which carries the source vapour towards the substrate. The CVD system is equipped with a vacuum system to evacuate other atmospheric gases present in the system. Vapour phase assisted technique is adopted for the synthesis of Zn:ZnO and ZnO films. In this technique, a smaller tube with one end closed is placed inside the bigger tube of CVD furnace. The source material is kept in a ceramic boat at higher temperature zone and the substrate is paced at lower temperature zone. Source is kept at the closed end of the smaller tube and the substrate is kept near the open end and the smaller tube is placed inside the bigger tube such that the closed end faces the upstream of the inert gas flow. The higher temperature of source material creates vapour and because of the closed end, a high pressure zone is created at this end of the tube. Substrate temperature is lower and because of the open end at this zone, a smaller pressure is developed. This pressure difference leads the flow of source material from the higher to lower temperature segment of the furnace and facilitates the deposition on the surface. The gold deposited on silicon has lower eutectic temperature (~375 °C) and temperature higher than this eutectic temperature allows the gold to form droplet on the silicon surface. The vapour of source material is deposited on these droplets and upon saturation the materials starts deposited on the surface in solid form leading the gold to either stay at the bottom of material or at the top. The whole process is summarized by vapour source depositing on liquid gold surface and leading to deposition of solid thin film. Hence, the process is termed as VLS process. Zinc oxide has higher melting point and hence it cannot be used alone as the source material for ZnO deposition hence, high purity graphite flakes are mixed with ZnO to bring the melting temperature down. This process is known as carbothermal process. The well mixed graphite flakes with ZnO acts as localized heating centres and helps in reducing the melting temperature of ZnO.

The source materials for ZnO thin film depositions are ZnO powder (99.99%, Alfa Aeser) and graphite flakes (99.8%, Alfa Aeser) in weight ratio of 1:4. Further, for Zn:ZnO thin films, additional source precursor which is zinc powder (99%, Alfa Aeser) in the weight ratio of Zn:ZnO:Graphite as 4:1:4. These materials are well mixed for 12 hours in ball milling system rotating with 1000 RPM. 03 g of these source materials are used each time for the respective experiment to deposit ZnO and Zn:ZnO thin film samples. Size of the silicon substrate used for each deposition is 1 cm x 1 cm and the separation between source material and substrate is maintained ~20 cm for each deposition.

The tube is placed inside the CVD with proper couplers for gas in and out system. The CVD is initially evacuated to 10^{-3} Torr to remove any residual gases present inside the tube. The source temperature is kept at 1050 °C at a ramp rate of 400 °C/hr. The substrate temperature is kept at 450 °C with ramp rate 152 °C/hr so that the source and substrate peak temperatures reach the respective peak values at the same time. The schematic diagram of the thermal CVD furnace is presented in figure 4.1.

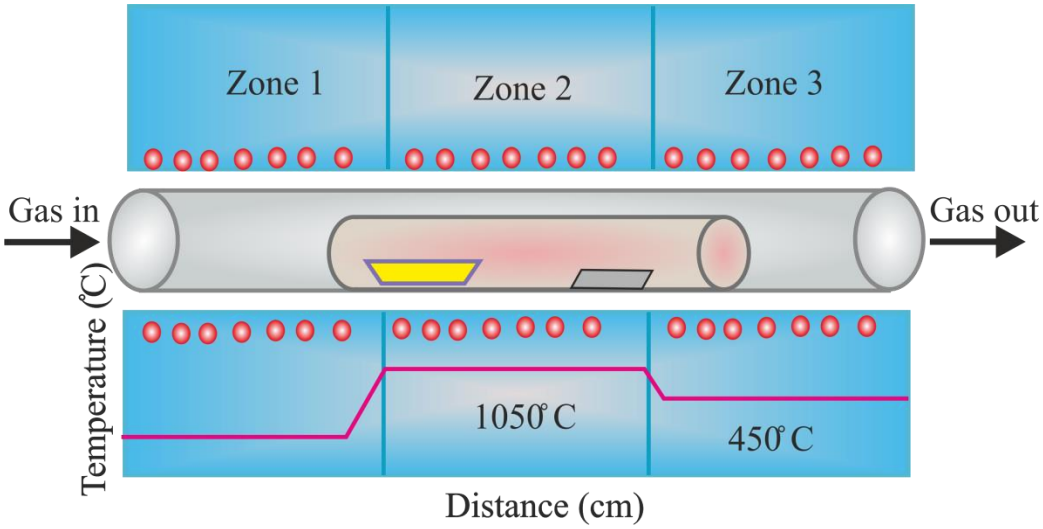

Figure 4.1 : Schematic of a double tube CVD system presented with respective growth temperature of different zones

The pressure of gas cylinder is maintained at 35 Torr and argon flow is maintained constant at 70 sccm for all depositions. The deposition time for both the films is 80minutes. The films are then cooled down at room temperature at natural rate and then taken out for further characterization. The gold is used as a catalyst to facilitate VLS growth as well as nanostructures but longer deposition time in our case has resulted in thin film structures of both the samples.

4.3 Results and Discussion

4.3.1 Structural and Microstructural

Crystallographic and structural information of these samples are analysed by XRD techniques. The X-ray diffraction patterns are presented in Figures 4.2 (a & b) for ZnO and Zn:ZnO, respectively. The obtained XRD pattern matched well with wurtzite structure of ZnO (ICDD no. 036-1451) without any impurity peaks substantiating the formation of pure phase ZnO. The pattern also shows that the natures of deposited films are polycrystalline. The lattice parameters of the samples are estimated using the formula

$$\frac{1}{d^2} = \left(\frac{4}{3}\right)\left(\frac{h^2 + hk + k^2}{a^2}\right) + \left(\frac{l^2}{c^2}\right) \qquad (4.1)$$

Where d is spacing between planes; h, k and l are Miller indices; a and c are lattice parameters of unit cell(Kumari et al., 2018a). The estimated lattice parameters for deposited ZnO (Zn:ZnO) thin films are a=3.183 Å (3.185 Å) and c=5.199 Å (5.202 Å). These values matched well with the reported lattice constants of ZnO. Orientation of Zn:ZnO is relatively enhanced along (002) direction in comparison to ZnO thin film. Williamson and Smallman's formula is used to calculate dislocation line densities δ of both the samples using formula $\delta = \frac{1}{D^2}$; where $D = \frac{0.94*\lambda}{B\ Cos\ \theta}$ is crystallite size (Kumari et al., 2018a) (Williamson and Smallman, 1956). The strain in the

samples are estimated using formula $\varepsilon = \frac{B\,cot\theta}{4}$; where θ is diffraction angle and B is full width half maximum (FWHM). Further, texture coefficients of the synthesized thin films are calculated as

$$TC(h\,k\,l) = \frac{\frac{I\,(h\,k\,l)}{I_0\,(h\,k\,l)}}{N^{-1}\sum\frac{I\,(h\,k\,l)}{I_0\,(h\,k\,l)}} \quad (4.2)$$

where, I is calculated and I_0 is standard X-ray intensity, referenced from ICDD# 036-1451 file of ZnO (Kumari et al., 2018a). The various estimated parameters of crystallographic information of these samples are provided in Table 4.1. The X-ray pattern of Zn:ZnO thin films showed that it has relatively better preferred orientation along (002) plane i.e. C-axis. Here, extra zinc atom should go to either antisite or interstitial position, as discussed earlier section. Since antisites have higher formation energy hence this is not favorable and formation of zinc interstitials is supported. Also, oxygen has larger ionic radii (1.4 Å) in comparison to zinc radii and antisite formation would have resulted in shrinkage of ZnO lattice because of smaller radius of zinc atoms. Hence, nearly equal calculated lattice parameters of both the samples omit the possibility of formation of antisite and substantiate the realization of zinc interstitials. There are two voids where these interstitials atoms can reside namely, tetrahedral and octahedral voids. The size of tetrahedral void is smaller to zinc interstitial atoms hence presence of Zn interstitials may cause instability. On the other hand, the size of octahedral void is comparable to interstitial atoms and hence this position will be favorable to zinc interstitials.

Changes in few crystallographic properties of Zn:ZnO are observed in comparison to pristine ZnO which can be seen from table 4.1. The crystallite size of Zn:ZnO sample has increased and the dislocation density of the sample has decreased with respect to ZnO. Texture coefficient of Zn:ZnO has increased with simultaneous decrease in strain of the Zn:ZnO sample.

Table 4.1 Different Structural Parameters for ZnO and Zn:ZnO Thin Film

Sample	2θ (degree)	FWHM (degree)	a (Å)	c (Å)	Crystallite size (nm)	Dislocation density (δ x 10^{15}) (line m^{-2})	Strain (ε x 10^{-3})	Texture coefficient
ZnO	34.42	0.258	3.183	5.199	33.68	8.81	3.6	2.4
Zn:ZnO	34.46	0.247	3.185	5.202	35.16	8.01	3.4	3.0

Morphological studies of these films are carried out using SEM in conjunction the elemental compositions of the samples are investigated by EDS. The SEM images along with EDS pattern in the insets are shown in figure 4.2 (c & d). The surface morphology of these thin films suggests that both have microstructured morphology on the surface. The grains of ZnO thin film are much smaller ~ 1.2 μm in comparison to Zn:ZnO films ~ 3.0 μm. Also, Zn:ZnO films morphology showed that the grains are having hexagonal tips pointing upwards. The zoomed hexagonal tips are shown in the inset of figure 4.2 (d). This result is in accordance with the results of XRD which substantiated a preferred orientation of Zn:ZnO film along c-axis. In contrast, grains of ZnO are randomly oriented. These microstructures are almost uniformly distributed across the whole film.

The EDX measurements on these samples indicate that zinc and oxygen atoms are present and both ZnO and Zn:ZnO samples have nearly equal oxygen atomic fraction. However, relatively lower atomic percentage of zinc in ZnO ~ 45.76% is observed with respect

to Zn:ZnO thin films ~51.76%. Presence of more zinc atom in Zn:ZnO film is assigned to the excess zinc which was used along with other source materials. Relatively larger zinc concentration in Zn:ZnO substantiates the presence of interstitial zinc.

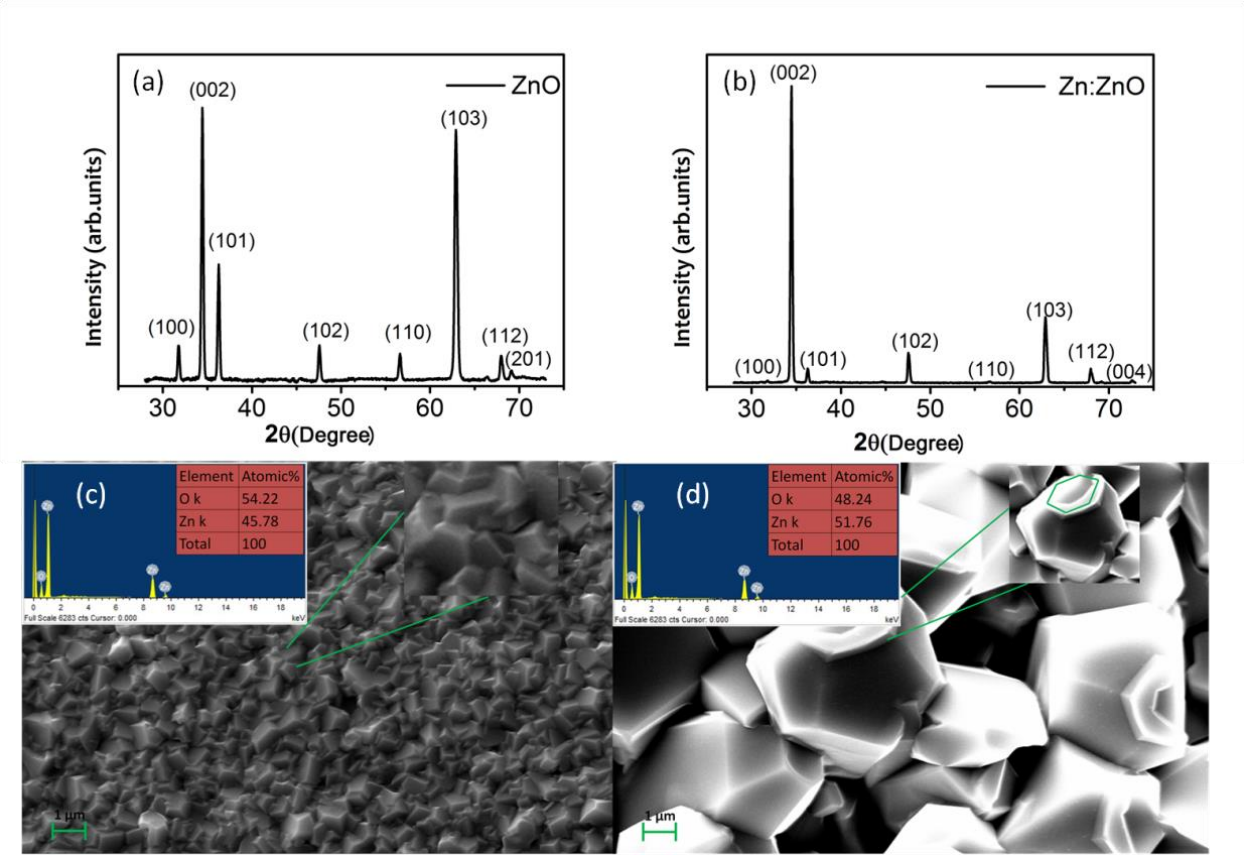

Figure 4.2: XRD for (a) ZnO, (b) Zn:ZnO ; SEM and EDX images with orientations in insets for (c) ZnO and (d) Zn:ZnO films

The topographical and surface properties are also investigated by AFM technique on 10 µm x 10 µm area of both the samples. The morphological studies of the samples are in accordance with the results obtained from SEM. The calculated average and RMS roughness of the ZnO films are 76 and 95 nm, respectively. The average and RMS roughness for Zn:ZnO is 187 nm and 235 nm, respectively. The AFM images are presented for ZnO and Zn:ZnO in figure 4.3 (a&b), respectively.

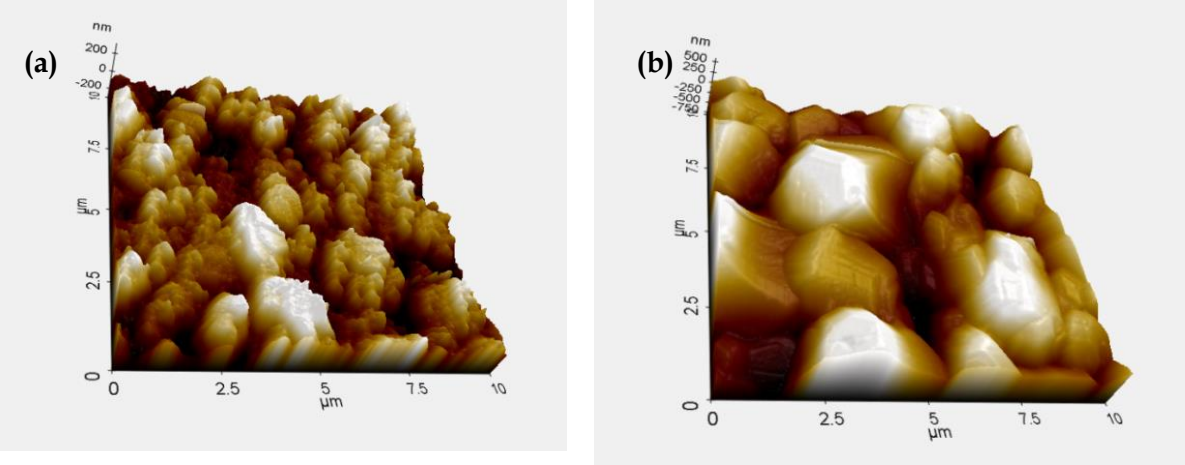

Figure 4.3: AFM images of (a) ZnO and (b) Zn:ZnO

4.3.2Optical Analysis

Raman spectroscopic measurements are carried out to understand the vibrational properties of as synthesized films at room temperature. Zinc oxide has hexagonal wurtzite structure and belongs to p63mc space group. It contains two formula units in a primitive cell and each primitive cell has four zinc oxide atoms which leads to 12 phonon modes in which 9 modes are optical and 3 modes are acoustic (Damen et al., 1966). The group theoretical analysis suggests that optical phonons of ZnO at Γ point (centre of Brillouine zone) are represented by the equation $\Gamma opt = A_1 + 2B_1 + E_1 + 2E_2$. Here, A_1 and E_1 are polar phonon modes and hence these modes are Raman as well as IR active. These polar modes are divided into longitudinal optical (LO) and transverse optical (TO) phonon modes having two different frequencies. Mode B_1 is Raman silent and not noticed in ZnO Raman spectra. Mode E_2 is non-polar and Raman active with two frequencies, $E_2^{(high)}$ and $E_2^{(low)}$; where they represent oxygen and zinc sublattice vibrations, respectively (Damen et al., 1966). Polar phono modes A_1 and E_1 are parallel polarized and perpendicular to the c-axis. The Raman spectra of ZnO and Zn:ZnO thin film samples are shown in figure 4.4 (a&b), respectively. Both the films showed a strong Raman peak at 99 cm^{-1} which represents $E_2^{(low)}$ phonon mode. This mode is a characteristic signature of zinc sublattice vibration. Another mode is observed at 438 cm^{-1} for both the films which is assigned to $E_2^{(high)}$ mode and it is a characteristic of oxygen sublattice vibration. Presence of strong $E_2^{(high)}$ mode substantiates presence of hexagonal wurzite structure and good crytsallinity of the films (Jothilakshmi et al., 2009). The intensity ratios ($I_{E2\ (low)}$/ $I_{E2\ (high)}$) are ~1.38 and 1.80 for ZnO and Zn:ZnO thin film samples, respectively. Relatively higher intensity ratio of Zn:ZnO in comparison to ZnO indicates that excess zinc is contributing towards the increased intensity $E_2^{(low)}$ modes. Adittionally, Zn:ZnO also showed a forbidden mode at 333 cm^{-1} which is assigned to second order peak of Raman scattering (Jothilakshmi et al., 2009). This mode is observed in resonance conditions and referred as zone boundary phonon, represented by difference of wavenumbers of $E_2^{(high)}$ and $E_2^{(low)}$ modes and is originated from crytsal distrubances. This disturbance in crystal may be observed due to excess zinc present in the system as this mode is not observed in ZnO thin film. Zn:ZnO also showed a broad and weak phonon modes at 379 and 575 cm^{-1}, which resemble A_1 (TO) and A_1 (LO) modes, respectively. These modes are often assigned to the presence of oxygen vacancies or zinc interstitials point defects (Jothilakshmi et al., 2009). Hence, presence of these modes in Zn:ZnO film supports the presence of zinc interstitials as these modes are not observed in ZnO films. There are few other peaks present at 300 cm^{-1}, 475 cm^{-1}, and 520 cm^{-1} which are attributed to presence of phonons of silicon which is used as substrates for deposition of these films. The observed and reported Raman modes are presented in table 4.2.

Table 4.2: Reported Raman Modes (Cuscó et al., 2007) and Observed Raman Modes in ZnO and Zn:ZnO Thin Films

Observed Raman modes	*Reported Raman shift (cm−1)*	*Observed Raman shift (cm−1)*	*Present in ZnO*	*Present in Zn:ZnO*
$E_2^{(low)}$	99	99	✓	✓
$E_2^{(high)}$-$E_2^{(low)}$	333	333	×	✓
A_1(TO)	378	379	×	✓
E_1(TO)	410	-	×	×

$E_2^{(high)}$	438	438	✓	✓
$A_1(LO)$	574	575	×	✓
$E_1(LO)$	590	-	×	×

Room temperature PL spectra of both the films are shown in figure 4.4 (c). Both ZnO and Zn:ZnO showed two peaks in the PL spectra, corresponding to UV (~375 nm) and visible region (~500 nm). The strong and sharp peak is observed at 376.66 nm and 379.77 nm for ZnO and Zn:ZnO, respectively. This emission peak is known as near band edge emission and is attributed to recombination of excitons i.e. band to band recombination of photo generated electrons and holes. The band gaps of the samples are calculated by NBE wavelength and observed values are almost same ~ 3.28 eV ± 0.02 eV for both the thin films. The weak emission band centred at 500 nm for both the samples is attributed to the recombination from point defects i.e. oxygen vacancies or zinc interstitials, present in the samples (Shan et al., 2005). It is observed from PL spectra that the intensity of defect mediated PL peak in visible region is relatively higher for Zn:ZnO sample with respect to ZnO indicating higher defect density, which is attributed to zinc interstitials present in the system.

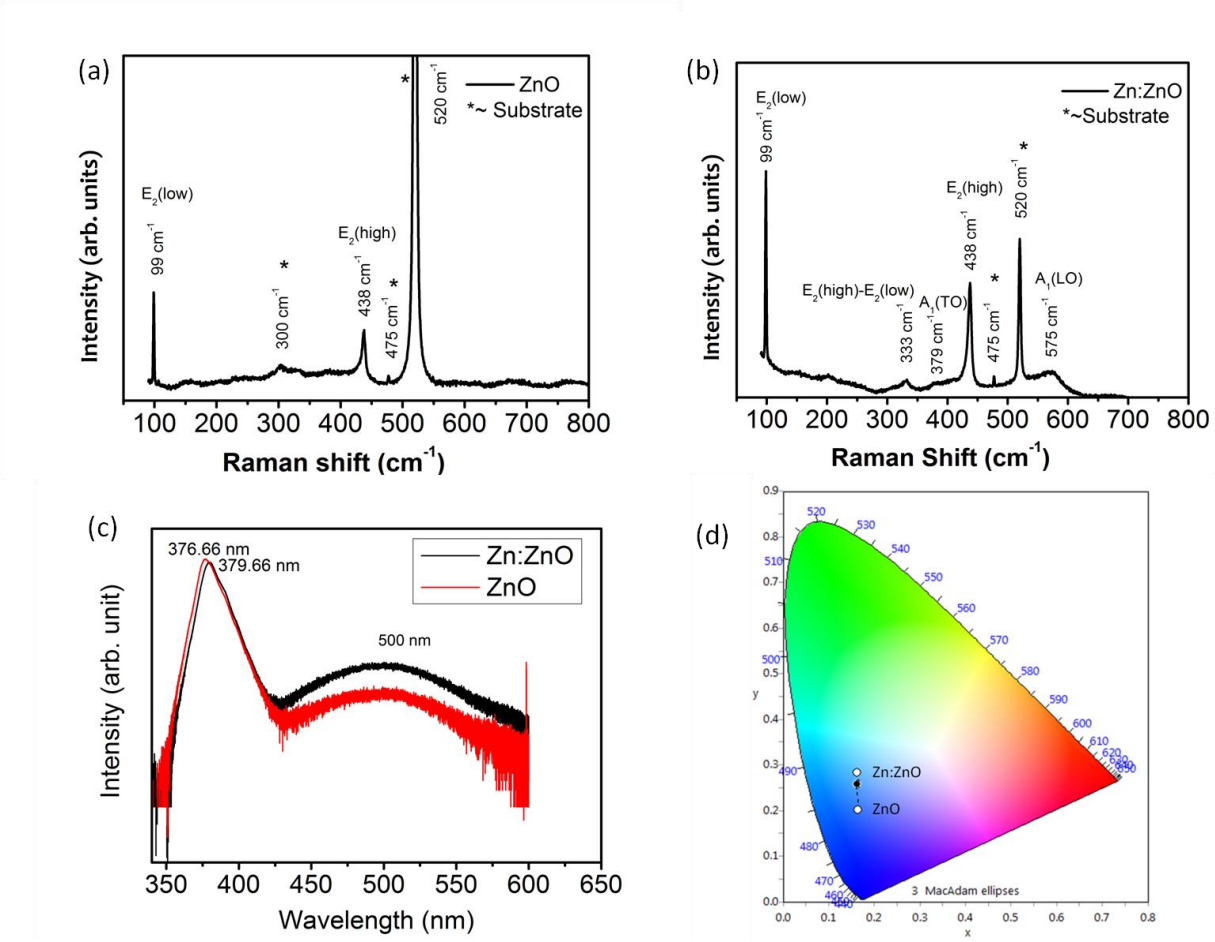

Figure 4.4: Raman spectra for (a) ZnO and (b) Zn:ZnO, (c) PL spectra for ZnO and Zn:ZnO and (d) Color emission spectra for ZnO and Zn:ZnO

Further, luminescence properties of the samples are correlated to the fluorescent characteristics by using CIE 1931 colour calculator (Vempati et al., 2012). For that, PL spectra of the samples are transported to the CIE- 1931 standard color calculator which is shown in figure

4.4 (d). A dark blue colour is perceived from ZnO samples and the observed chromatic coordinates for ZnO thin film are (0.164, 0.200) figure 4.4(d). The perceived colour for Zn:ZnO film is light blue with chromatic coordinates (0.162, 0.282). This considerable shift in chromatic coordinates in Zn:ZnO to ZnO suggests that excess zinc interstitials is contributing in fluorescent properties of Zn:ZnO films.

4.3.3 Electrical Characterization

The current-voltage (I-V) measurements are performed in metal-insulator-metal (MIM) configuration using circular silver contact with 1 mm diameter and at ~ 1 mm separation. The I-V results of the samples are measured by applying sweeping voltage bias from -5 to 5 V between the electrodes. The measured I-V characteristics for ZnO and Zn:ZnO thin film samples are presented in Figure 4.5 (a & b), respectively. The measurements suggest that the contacts are ohmic and the observed peak currents are 80 µA and 20 mA for ZnO and Zn:ZnO thin films at 5 V, respectively. The observed peak current of Zn:ZnO is large and it is assigned to presence of zinc interstitial atoms as shallow donors, thus, providing electrons to CB, and leading to large current.

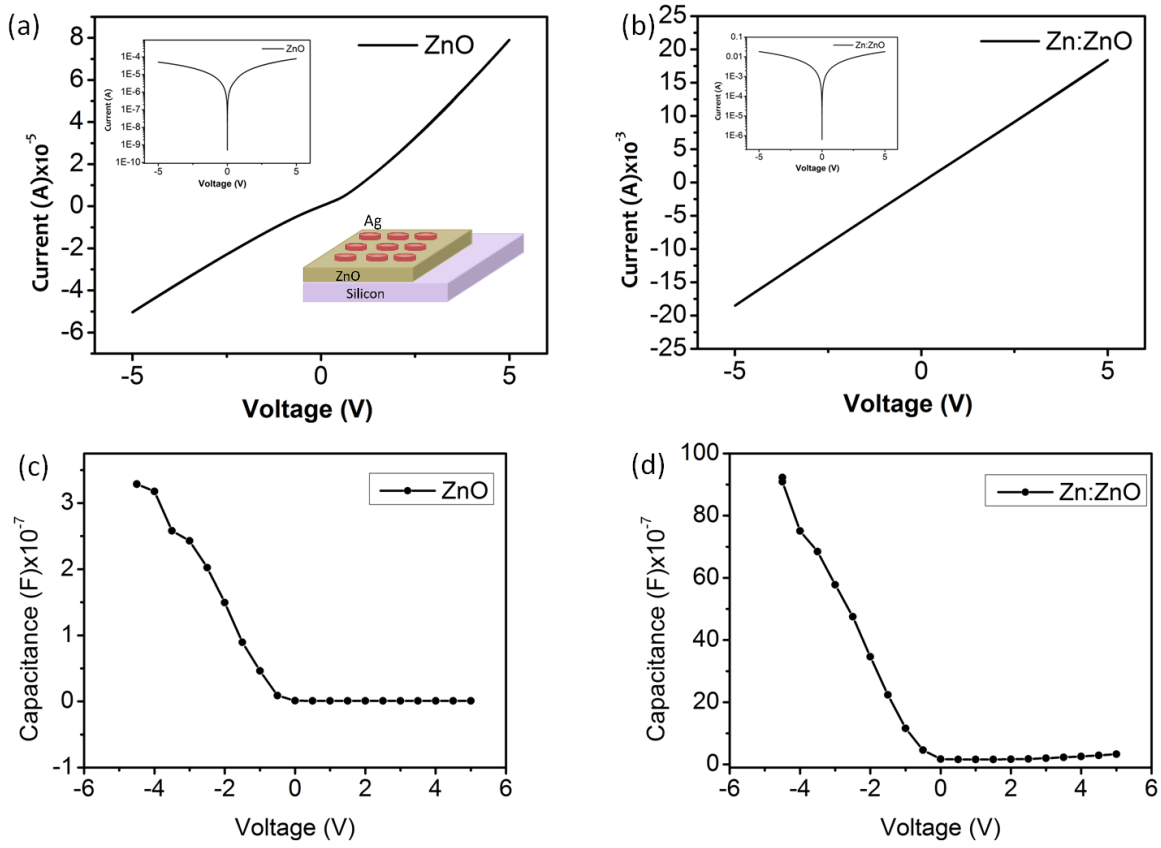

Figure 4.5: I-V response for (a) ZnO and (b) and Zn:ZnO ; C-V response for (c) ZnO and (d) Zn:ZnO

The capacitance-voltage (C-V) measurements are carried out using MIM capacitor configuration, where silver is top contact deposited on the films and highly doped n-type silicon substrate as the bottom contact. The measurements are carried out at 10 kHz and the observed C-V results for ZnO and Zn:ZnO films are given in Figure 4.5 (c & d), respectively. The measured capacitance at 5 V for ZnO and Zn:ZnO films are ~ 3.4×10^{-7} F and ~ 9×10^{-6} F, respectively.

The carrier concentrations of the films are estimated using Mott-Schottky (M-S) analysis. The M-S graph ($1/C^2$ and voltage) is derived from the observed C-V data. The M-S plots for ZnO and Zn:ZnO thin films are given in Figure 4.6 (a & b), respectively.

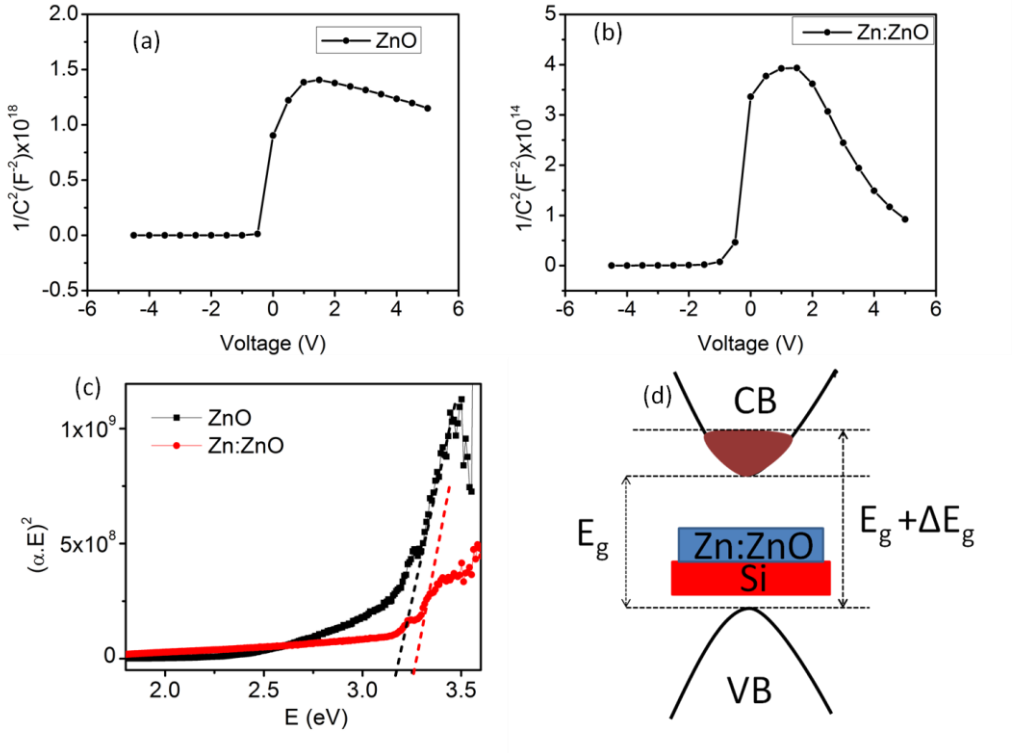

Figure 4.6: M-S graphs for (a) ZnO (a) and (b) Zn:ZnO; band gap graphs for (c) ZnO and Zn:ZnO and (d) Schematic diagram of B-M shift in Zn:ZnO thin films

The effective carrier concentrations are extracted from the linear slop of Mott-Schottky (M-S) curves of the samples as

$$N_d = -\frac{2}{(q\varepsilon_0\varepsilon_r A^2)*\left[\frac{d\left(\frac{1}{c2}\right)}{d(v)}\right]} \quad (4.3)$$

where, q is charge of the electron, ε_0 is permittivity of vacuum, ε_r (=10 for ZnO[46]) is permittivity of medium, A is the electrode area and d $(1/c^2)/d$ (v) is the linear region of slope of the M-S curve (Kumari et al., 2018a) (Shan et al., 2005). The positive slope of the linear portion indicates that the films have n-type conductivity. The calculated carrier concentrations of ZnO and Zn:ZnO thin film samples are ~ $7.5x10^{15}$ cm^{-3} and ~ $6x10^{19}$ cm^{-3}, respectively. The calculated carriers are four order of magnitude higher for Zn:ZnO films than the ZnO film. This enhancement in carrier concentration of Zn:ZnO in comparison to ZnO is assigned to zinc interstitials which acts as shallow donor and hence provides more electrons to the conduction band.

The presence of excess carrier may cause a shift in band gap which is known Burstein-Moss (B-M) shift by filling the top layer of conduction band. This is resulted by shifting of quasi Fermi level inside the CB of the semiconductor. The relation between shift in energy band gap and carrier concentration is given by

$$\Delta E_g = \left(\frac{h^2}{8\Pi^2 m^*}\right)(3\Pi^2 n)^{2/3} \quad (4.4)$$

where m* (0.38 for ZnO) is effective mass of the electron, n is the carrier density and h represents Planck constant (Kumari et al., 2018a) (Cebulla et al., 1998). The calculated B-M shift for Zn:ZnO i.e. ΔE_g is ~ 0.13 eV The band gap of Zn:ZnO is 0.13 eV higher than ZnO thin film, as observed from the optical measurements, figure 4.6 (c). The observed results substantiates

that band gap of Zn:ZnO is higher than ZnO thin film by 0.1 eV verifying the results obtained from BM shift. The schematic diagram of BM shift is given in Figure 4.6 (d).

4.4 Conclusion

In conclusion, ZnO and Zn:ZnO thin films are synthesized by simple carbothermal assisted vapor phase transport technique by utilizing a thermal CVD system. Structural analysis of the samples by XRD analysis substantiates that Zn:ZnO thin films are relatively more crystalline as well as C-axis oriented than ZnO thin film. The studies also revealed that excess zinc might occupy octahedral interstitial position in ZnO lattice. The EDS measurements revealed that Zn:ZnO have relatively higher atomic concentration of zinc that ZnO sample substantiating the presence of interstitial zinc atoms. Raman and PL measurements further verified that excess zinc is present in the Zn:ZnO film and may be acting as interstitial point defect. The fluorescent characteristics obtained from CIE 1931 color calculator revealed the excess interstitial zinc atoms are shifting the colour coordinate for Zn:ZnO sample towards light blue region. The electrical characterization of Zn:ZnO sample reveals BM shift ~ 0.13 eV, substantiating the existence of zinc interstitial shallow donors. Hence, this study provide the information about contribution of Zn interstitial defects in light emission which might be beneficial for controlling electrical properties of ZnO thin films for desired applications.